Title

Evaluating the uncertainty of Landsat-derived vegetation indices in quantifying forest fuel treatments using bi-temporal LiDAR data

Authors

Ma, Qin
Su, Yanjun
Luo, Laiping
et al.

Publication Date

2018-12-01

DOI

10.1016/j.ecolind.2018.07.050

Peer reviewed

Ecological Indicators 95 (2018) 298–310

Contents lists available at ScienceDirect

Ecological Indicators

journal homepage: www.elsevier.com/locate/ecolind

Evaluating the uncertainty of Landsat-derived vegetation indices in quantifying forest fuel treatments using bi-temporal LiDAR data

Qin Ma[a], Yanjun Su[a,b,*], Laiping Luo[a], Le Li[c], Maggi Kelly[d,e], Qinghua Guo[a,b]

[a] Sierra Nevada Research Institute and School of Engineering, University of California, Merced, CA, USA
[b] State Key Laboratory of Vegetation and Environmental Change, Institute of Botany, Chinese Academy of Sciences, Beijing, China
[c] School of Geography, South China Normal University, Guangzhou 510631, China
[d] Department of Environmental Sciences, Policy and Management, University of California, Berkeley, CA 94720-3114, United States
[e] University of California, Division of Agriculture and Natural Resources, United States

ARTICLE INFO

Keywords:
Forest fuel treatment
Vegetation index
Aboveground biomass
LiDAR

ABSTRACT

Forest ecosystems in the American west have long been influenced by timber harvests and fire suppression, and recently through treatments that reduce fuel for fire management. Precisely quantifying the structural changes to forests caused by fuel treatments is an essential step to evaluate their impacts. Satellite imagery-derived vegetation indices, such as the normalized difference vegetation index (NDVI), have been widely used to map forest dynamics. However, uncertainties in using these vegetation indices to quantify forest structural changes have not been thoroughly studied, mainly due to the lack of wall-to-wall validation data. In this study we generated forest structural changes in aboveground biomass (AGB) and canopy cover as a result of fuel treatments using bi-temporal airborne light detection and ranging (LiDAR) data and field measurements in a mixed coniferous forest of northern Sierra Nevada, California, USA. These LiDAR-derived forest structural measures were used to evaluate the uncertainties of using Landsat-derived vegetation indices to quantify treatments. Our results confirmed that vegetation indices can accurately map the extents of forest disturbance and canopy cover changes caused by fuel treatments, but the accuracy in quantifying AGB changes varied by the pre-treatment forest densities and treatment intensity. Changes in vegetation indices had relatively weaker correlations (coefficient of determination < 0.45) to biomass changes in forests with sparse (AGB < 100 Mg/ha) or dense biomass (AGB > 700 Mg/ha), than in forests with moderate-density (AGB between 100 Mg/ha and 700 Mg/ha) before the disturbances. Moreover, understory treatments (canopy height < 10 m) were poorly indicated by changes in satellite-derived vegetation indices. Our results suggest that when relating vegetation indices to AGB changes, researchers and managers should be cautious about their uncertainties in extremely dense or sparse forests, particularly when treatments mainly removed small trees or understory fuels.

1. Introduction

Selective removal of forest fuels (i.e. fuel treatment) is a widely used forest management and restoration practice with both economic and ecological goals (Agee and Skinner, 2005; Kerr and Haufe, 2011; Mitchell et al., 2009; Park et al., 2018). In the Sierra Nevada, California, forest fuel treatments including logging, thinning, and mastication have been conducted for many years (Knapp et al., 2013). The United States Department of Agriculture Forest Service (referred to as USFS hereafter) spent 52% of its annual budget on wildfire suppression and management in fiscal year 2015, and this percentage is expected to increase in the coming decades (Stephens et al., 2016a, 2018). These long-term and broad-area treatments have significantly altered tree species and age composition, as well as forest landscape structures (Agee and Skinner, 2005; Collins et al., 2011a; Mitchell et al., 2009; Parsons and DeBenedetti, 1979). Consequently, forest ecosystem services and ecological functions have also changed, including forest carbon stock, vegetation water use, wildlife habitat, and forest fire frequency and severity (Bales et al., 2011; Battles et al., 2001; Stephens et al., 2009; Tempel et al., 2014). Because these management practices are so impactful on forest structure, accurate measurement of the changes to forest structure as a result of fuel treatments is necessary, but doing so remains challenging.

Accurate and timely quantification of forest changes in abundance, production, and spatial pattern is a necessary step for forest fuel treatment evaluation (Huang et al., 2009; Su et al., 2016a). Traditional

* Corresponding author at: Institute of Botany, Chinese Academy of Sciences, China.
E-mail addresses: qma@ucmerced.edu (Q. Ma), suyanjun1987@gmail.com (Y. Su), maggi@berkeley.edu (M. Kelly).

https://doi.org/10.1016/j.ecolind.2018.07.050
Received 15 May 2018; Received in revised form 22 July 2018; Accepted 24 July 2018

forest fuel treatment evaluation has relied heavily on in-situ measurements of tree height, diameter at breast height (DBH), tree density, and distribution (Collins et al., 2015; Knapp et al., 2013). Due to the high cost of field measurements in both time and labor, forest inventory data were often limited to selected plots or transects. When these local measures are scaled to landscapes or regions with auxiliary data, large uncertainties can be introduced (Schroeder et al., 2014).

Remote sensing techniques have been widely used in forestry to map and monitor forest dynamics (Cohen et al., 2016; Hansen et al., 2013; Schroeder et al., 2011; White et al., 2016, 2017). The applications of optical satellite imagery in forestry have increased dramatically at both temporal and spatial scales, particularly in the recent decade, with open access to Landsat satellite imagery (Schroeder et al., 2017; Vogelmann et al., 2017; Wang et al., 2016; White et al., 2017; Wulder et al., 2012a). A number of satellite imagery-derived vegetation indices, such as normalized difference vegetation index (NDVI), normalized difference water index (NDWI), and normalized burn ratio (NBR) have been developed to monitor forest dynamics. Among them, NDVI has demonstrated to be a strong indicator of vegetation greenness, biomass and water use, and has been widely used to quantify forest disturbances and their recoveries (Gamon et al., 1995; Tucker, 1979; Veraverbeke et al., 2012; Viedma et al., 1997). NBR, a combination of the near infrared and short wave infrared bands, has many applications for forest disturbance detection, but is mainly emphasized for forest fire severity mapping (Key and Benson, 2006; Miller and Thode, 2007). The Tasseled Cap Transformation (TCT) is another widely applied method for quantifying the vegetation vigor, coverage, and density by extracting the greenness, brightness, and wetness of the land surface from multispectral satellite imagery (Crist, 1985; Crist and Cicone, 1984; Huang et al., 2002). The Tasseled Cap Angle (TCA), calculated from the ratio of greenness and brightness components in the TCT, has been successfully used to characterize the spatio-temporal forest dynamics in northwestern Alberta, Canada (Gómez et al., 2011). Although these vegetation indices were widely used to map forest dynamics, their accuracies in quantifying change in forest structures, such as canopy cover and biomass, have not been fully studied. Some issues with these applications have been reported in previous studies. For example, the saturation effect of vegetation indices, like NDVI, may cause its failure to indicate the increase or decrease of structure parameters, such as aboveground biomass (AGB) in forests with extremely high density and large biomass, and thus may lead to the underestimation of forest treatment (Gamon et al., 1995; Gao et al., 2000; Mutanga and Skidmore, 2004). Moreover, shadows in mountainous areas and cloud cover in satellite imagery may result in the spatio-temporal variations in vegetation indices, which are unnecessarily related to forest disturbances (Kennedy et al., 2010; Verbyla et al., 2008; Zhu and Woodcock, 2012). A systematic evaluation of these uncertainties is necessary to precisely assess the impacts of forest fuel treatments. However, these evaluations are challenging, mainly due to the lack of accurate and timely ground reference data for validation.

Light detection and range (LiDAR) is an active remote sensing technique which can characterize three-dimensional forest structure parameters with high accuracy (Coops et al., 2007; Kelly and Di Tommaso, 2015; Næsset and Økland, 2002). Laser pulses emitted by LiDAR sensor can penetrate through the forest canopy, and therefore, are less impacted by the shadowing or saturation effects (Ma et al., 2017a; Su et al., 2016a). Airborne LiDAR data combined with field measurements have been successfully applied to map tree height (Næsset, 1997; Næsset and Bjerknes, 2001), large tree density(Kramer et al., 2016), crown base height (Popescu and Zhao, 2008), canopy cover (Korhonen et al., 2011; Ma et al., 2017a), leaf area index (Korhonen and Morsdorf, 2014; Zheng and Moskal, 2009), fire-related forest stand structure metrics (Blanchard et al., 2011; Jakubowksi et al., 2013; Kelly et al., 2017; Kramer et al., 2014), and aboveground biomass (AGB) (Dalponte et al., 2018; Li et al., 2015; Luo et al., 2017; Su et al., 2016b; Tao et al., 2014; Zhao et al., 2012) from the individual tree to forest stand scale. LiDAR data have been increasingly used as an alternative or auxiliary data source in forest inventory (Korhonen et al., 2011; Wulder et al., 2012b). With continued accumulation of LiDAR data over time and space, studies focusing on detecting and monitoring forest structure changes from multi-temporal LiDAR data have increased in the recent years (Ma et al., 2017b; McCarley et al., 2017; Su et al., 2016a; Zhao et al., 2017). These successful applications demonstrated the strong potential of using airborne LiDAR, combined with field measurements, to provide a wall-to-wall validation data for evaluating the accuracies of satellite imagery-based quantification of forest structure dynamics.

The objective of this study is to systematically assess the uncertainties of satellite imagery-based vegetation indices in characterizing fuel treatment-induced forest structural changes. The uncertainty analysis focused on the capabilities of Landsat-derived vegetation indices in quantifying the forest structural changes, resulted from fuel treatments conducted at various intensities over different forest densities. LiDAR data and field measurements derived forest structural changes, primarily in AGB and canopy cover, were used as ground references to evaluate the performances of four widely used Landsat-derived vegetation indices in detecting and quantifying forest fuel treatment in a conifer-dominated forest in the Sierra Nevada, California. Results from this study can help to understand the effectiveness of and uncertainties related to Landsat-derived vegetation indices in forest treatment quantification and to provide guidance for forest management and monitoring.

2. Materials and methods

2.1. Study area

The study site (39° 07′ N, 120° 36′ W) covers an area of 99.5 km^2 and locates within the Tahoe National forest of the Sierra Nevada, California. It is a mountainous area with the elevation ranging from 579 m to 2184 m above sea level (Fig. 1). This forest is dominated by five major tree species: white fir (*Abies concolor*), red fir (*Pseudotsuga menziesii*), incense cedar (*Calocedrus decurrens*), sugar pine (*Pinus lambertiana*), and ponderosa pine (*Pinus ponderosa*). Broadleaf trees and chaparral, primarily California black oak (*Quercus kelloggii*) and manzanita (*Arctostaphylos spp*), co-exist with the conifers, but in smaller numbers. The climate is Mediterranean with an annual total precipitation of 1661 mm/yr (averaged from water years from 2008 to 2013).

Fuel treatments were implemented in the study area as part of the Sierra Nevada Adaptive Management Project, which was designed to study how fuel treatments can affect fire risk, wildlife habitat, and the water cycle (Hopkinson et al., 2017; Saksa et al., 2017). The majority of the treatments were conducted between 2008 and 2013 within a treatment boundary proposed by the USFS (the blue boundary in Fig. 1). This area of forest was dominated by small to mid-sized conifers with relatively high density (approximately 67% of canopy cover before the treatment) as a result of long-term fire suppression before treatments (Tempel et al., 2015). The fuel treatments were designed to reduce ladder fuels, or the forest fuels that provide vertical fuel continuity and can preheat unignited canopy fuels in a fire (Kramer et al., 2016, 2014; Menning and Stephens, 2007). Thus, the treatments concentrated on mechanical thinning at selected locations (Collins et al., 2011b) and focused on low and mid-strata of canopy, with small to medium sized trees removed. The study area and fuel treatments provide a natural experiment to evaluate the effectiveness of Landsat-derived indices in quantifying forest structure in two ways. First, the complex terrain and fine-scale selective thinning likely provided a challenge for Landsat-derived vegetation indices to quantify structural changes, and second, the availability of detailed before and after treatment LiDAR data provided detailed reference data with which to evaluate the accuracies and uncertainties in measuring structure from Landsat.

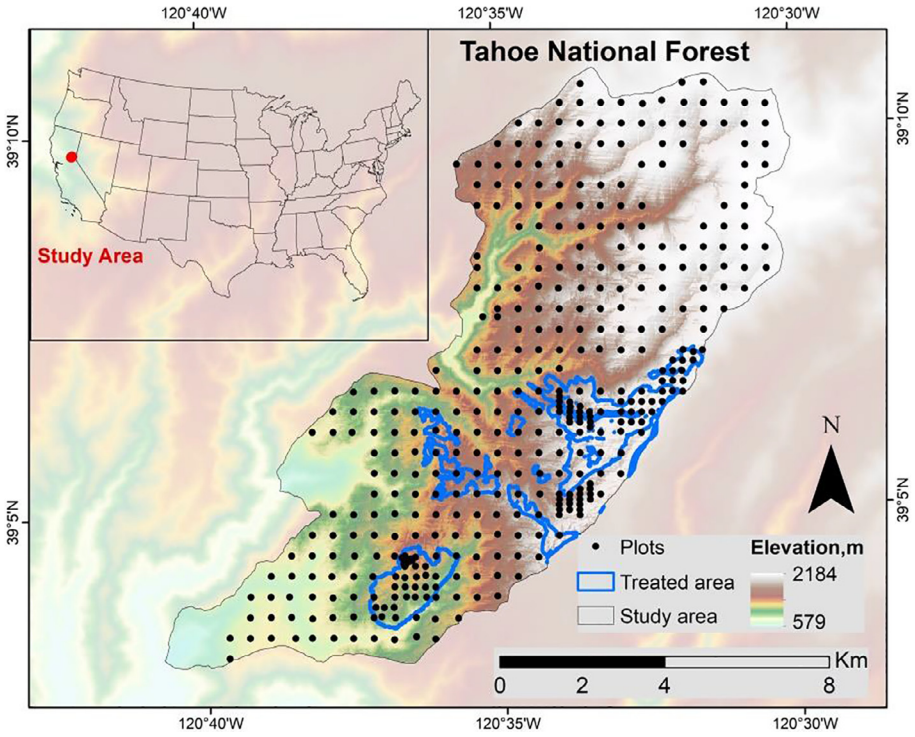

Fig. 1. The study area with the boundary of treated area proposed by the USFS. The locations of field measured plots are also shown on the map.

2.2. Data and methods

2.2.1. Field data

A total of 328 plots were surveyed in the field during the summer of 2008 and 2013 to characterize the forest structural changes from pre- to post-treatment. The plot distribution started from a random point and covered the entire study area in a 500 m spaced grid. The plot density was intensified (250 m or 125 m spacing) in two small instrumented catchments for hydrological studies. Each plot was in circular shape with an area of 500 m^2. In the pre-treatment (2008) plot survey, tree height, diameter at breast height (DBH), species, and height to live crown base were measured for individual trees in the plot, and the measurements of trees with a DBH larger than 5 cm were recorded. In the post-treatment (2013) survey, the DBH and tree height were re-measured for individual trees in the sampled plots (Table 1).

Plot-level aboveground biomass (AGB) was estimated using the Jenkins allometric equations (Jenkins et al., 2003) based on tree DBH. The total aboveground biomass for each individual tree was calculated following the general form in Eq. (1). Each species has specific equation coefficient (b_0, b_1).

$$ACB = \exp(b0 + b1ln(DBH)) \quad (1)$$

The AGB (Mg/ha) in the plot location was the sum of the total aboveground biomass over all field measured trees, and then divided by the area of the plot (500 m^2). Detailed coefficients for each species can be found in Jenkins et al. (2003). The same equations were applied to estimate the plot-level AGB for both pre- and post- treatments.

2.2.2. LiDAR data

An Optech GEMINI airborne laser terrain mapper system was used to acquire both pre- and post-treatment airborne LiDAR data within the study area. The pre- and post-treatment LiDAR data were collected in September 2008 and August 2013, respectively. The LiDAR data were collected with a 67% swath overlap. The flight heights were between 600 m and 800 m aboveground. The LiDAR sensor has a scanning frequency of 40–60 Hz and a scan angle of 12–14° on either side of nadir. It collected up to four discrete returns per shot. The final LiDAR point cloud had a total density of 10 points/m^2 and first return density of

Table 1
A summary of field measurements by tree species. Parameters include the number of trees, DBH, tree height from both pre- and post-treatment. The values are presented as mean ± standard deviation.

Tree Species	No. of trees		DBH, cm		Tree height, m	
	Pre	Post	Pre	Post	Pre	Post
White fir	3013	2250	25.49 ± 17.84	28.25 ± 19.25	12.80 ± 8.44	13.86 ± 9.48
Red fir	304	251	34.12 ± 19.49	33.88 ± 22.89	15.34 ± 10.10	14.99 ± 11.42
Incense cedar	568	452	26.39 ± 20.19	28.63 ± 21.68	10.59 ± 6.99	11.71 ± 7.83
Mountain dogwood	14	12	7.07 ± 1.7	8.17 ± 3.12	4.98 ± 1.07	6.30 ± 1.59
Live oak	53	40	11.63 ± 6.32	11.29 ± 4.37	5.96 ± 2.59	7.89 ± 4.8
Sugar Pine	691	558	38.36 ± 31.58	45.06 ± 33.12	17.49 ± 12.45	20.34 ± 13.36
Western white pine	16	11	24.63 ± 19.22	29.46 ± 21.66	10.3 ± 6.79	11.57 ± 8.38
Ponderosa pine	887	874	27.38 ± 20.33	27.96 ± 20.62	13.20 ± 8.97	13.85 ± 9.2
Douglas fir	1205	1061	28.27 ± 22.27	29.82 ± 22.30	15.25 ± 9.1	16.30 ± 10.05
Black oak	178	127	26.27 ± 18.93	24.18 ± 16.44	12.83 ± 6.21	11.32 ± 6.2
Sequoia	3	2	19.53 ± 15.76	33.8 ± 14.00	7.56 ± 6.88	13.55 ± 6.86

8.2 points/m^2 on average. A total of 800 ground GPS points were collected to calibrate the two airborne LiDAR flights as well as to assess the spatial accuracy. The spatial accuracy was similar between the two LiDAR datasets, with around 10 cm in horizontal and 5–35 cm in vertical.

Forest structure parameters, including AGB and canopy cover, were generated from the LiDAR data and field plot measurements for both pre-and post-treatment forest. First, The ground returns were classified from all LiDAR returns using a filter algorithm (Zhao et al., 2016) in LiDAR360 software. Then a digital terrain model (DTM) was generated from LiDAR ground returns at 1 m spatial resolution using the ordinary Kriging algorithm (Guo et al., 2010). The digital surface model was interpolated from the LiDAR first returns using a similar method as the DTM. The canopy height model (CHM) was then calculated as the difference between DSM and DTM for both pre- and post-treatment LiDAR data. The wall-to-wall AGB estimate was generated by applying the plot-level relationship between field measured AGB and LiDAR CHM metrics to the whole study area, as suggested in (Li et al., 2015; Ni-Meister et al., 2010). The details of AGB estimation are introduced in 2.2.3. The canopy cover was calculated directly from LiDAR data as the ratio of LiDAR first returns that were higher than the tree crown threshold (Ma et al., 2017a) within each statistic grid. We used the 2 m as the height threshold of tree crowns as it is a commonly used threshold to separate trees from non-tree vegetation (Ma et al., 2017a,b; Nilsson, 1996), and also suitable for this study site according to field measurements. For comparison, both AGB and canopy cover were calculated at the same spatial resolution as Landsat imagery (30 m by 30 m).

2.2.3. AGB estimations

The wall-to-wall vegetation AGB maps were estimated using plot-level relationships between LiDAR derived tree height metrics and field measured AGB. Various methods have been developed for AGB estimation from LiDAR data and field measurements (Valbuena et al., 2017), including linear regression (Li et al., 2015; Magnussen et al., 2015), exponential regression (Lim and Treitz, 2004), plot-aggregate allometry(Asner and Mascaro, 2014), and machine learning (Gleason and Im, 2012). Among them, the linear regression has advantages of simplicity and relatively low risk of overfitting, while being able to predict the majority of the variations in field-measured AGB, according to a comparison study conducted using the same pre-fire LiDAR dataset (Li et al., 2015). Therefore, in this study we implemented linear regression following the equation:

$$\mathrm{AGB} = aH^2 + bH + c \quad (2)$$

where H is the LiDAR-derived the mean tree height (the averaged CHM value within each plot), as suggested by Li et al. (2015); Ni-Meister et al. (2010); a, b, and c are coefficients regressed from plot-measurements and LiDAR metrics using the least-squares method. The linear regression models were generated for pre- and post-treatment independently and applied to the study area. For comparison, we resampled the AGB maps estimated from LiDAR and field measurements into 30 m resolution (referred as AGB maps, hereafter) and co-registered them to the satellite imagery. The AGB change was generated by subtracting post-treatment AGB map from pre-treatment AGB map for each pixel.

2.2.4. Satellite imagery

The pre- and post-treatment satellite images were obtained from Landsat-5 TM and Landsat-8 OLI sensors in 2008 and 2013, respectively. These surface reflectance images over the whole growing season (June 1st to October 1st) were collected from the high-level top-of-atmosphere product in Google Earth Engine (Gorelick et al., 2017). The pixels with cloud or snow cover were excluded from all images using the mask developed by (Zhu and Woodcock, 2012). A maximum-value composite (MVC) was applied to the annual images from both pre- and post-treatments. The MVC method composited the annual images by mosaicking the land-surface reflectance with the highest NDVI values for each pixel (Holben, 1986). Comparing to using single-date imagery, vegetation indices derived from MVC can better present variations in vegetation greenness and less likely to be influenced by the atmospheric effects or the difference in solar-sensor-geometry (Delbart et al., 2006). Moreover, we homogenized surface-reflectance from Landsat-5 TM to Landsat-8 OLI sensors using the regression-based method introduced in (Su et al., 2017; Sulla-Menashe et al., 2016). The MVC of Landsat-7 ETM+ surface reflectance images obtained in both pre- (2008) and post-treatment (2013) were calculated as a reference for sensor homogenization. We randomly selected 100 samples (1 km by 1 km) over the study area. Samples located in any black (no Landsat data) strip were moved 10 km in a random direction to avoid the impacts from the failed Landsat-7 ETM+ sensor on homogenization. The mean values of MVC of surface-reflectance images within each sample were used to build regression equations. These regression equations were then applied to calibrate the whole MVC images from Landsat-5 TM (2008) and Landsat-8 OLI (2013) into Landat-7 ETM+ in the corresponding years for better comparison in vegetation indices between pre- and post-treatment.

2.2.5. Vegetation indices calculation

Four vegetation indices were calculated to quantify structural changes resulting from fuel treatments. They were: normalized difference vegetation index (NDVI), normalized difference water index (NDWI), normalized burn ratio (NBR), and Tasseled Cap Angle (TCA). NDVI, NDWI, and NBR are based on normalized differences between two given surface-reflectance bands, which characterized the greenness (Tucker, 1979), wetness (Su et al., 2017), and the ratio between the photosynthesis vegetation and the bare ground (Miller and Thode, 2007), respectively (Eqs. (3)–(5)). The TCA was calculated as the angle formed by the greenness and brightness components (Gómez et al., 2011) derived from the Tasseled Cap Transformation of six surface-reflectance bands (Eq. (6)). All the four vegetation indices were generated from the homogenized MVC Landsat surface-reflectance images for both pre- and post-treatment. The differences in Landsat-derived vegetation indices (referred as vegetation indices, hereafter) between the post-and pre-treatment were compared with AGB changes.

$$\mathrm{NDVI} = (R_{nir} - R_{red})/(R_{nir} + R_{red}) \quad (3)$$

$$\mathrm{NDWI} = (R_{nir} - R_{swir1})/(R_{nir} + R_{swir1}) \quad (4)$$

$$\mathrm{NBR} = (R_{nir} - R_{swir2})/(R_{nir} + R_{swir2}) \quad (5)$$

$$\mathrm{TCA} = \arctan(TCT_{Greenness}/TCT_{brightness}) \quad (6)$$

where R_{nir}, R_{red}, R_{swir1}, R_{swir2} are homogenized MVC surface-reflectance in near infrared band, red band, shortwave infrared band 1, and shortwave infrared band 2, respectively. $TCT_{Greenness}$ and $TCT_{brightness}$ are the greenness and brightness components from the Tasseled Cap Transformation (Crist, 1985) of homogenized MVC surface-reflectance.

2.2.6. Comparison between vegetation indices and AGB maps

The accuracies and uncertainties of vegetation indices in quantifying forest biomass disturbances were evaluated by comparing them to LiDAR-derived AGB maps. First, we compared the changes of vegetation indices and AGB maps qualitatively, in terms of their spatial extents and distributions of detected changes. We then quantified the correlations between changes in vegetation indices and AGB maps at a pixel-level using the Pearson's correlation coefficients. The correlations were evaluated over three different regions: (1) within the USFS proposed treated boundary, (2) in the untreated area outside of the treatment boundary, and (3) over the entire study area, including both treated and untreated areas. The first two regions represented changes either driven by human treatment, or caused by natural disturbances, respectively; and the third region included changes induced by multiple

potential causes. The comparison among the three regions enabled us to evaluate the effectiveness of vegetation indices in quantifying changes induced by different sources.

To assess the capability of vegetation indices in quantifying biomass disturbances over forests with different densities, we categorized each region into seven pre-treatment AGB groups, and compared their correlations to AGB and canopy cover changes among groups. In addition to forest density, the differences in the height level where the treatment was conducted might also influence the usefulness of vegetation indices. To evaluate this influence, we classified the treated area into four height classes determined by the level where the majority of forest structural loss occurred. The four height strata were defined as: 1–5 m, 5–10 m, 10–20 m, > 20 m, which represented the small tree/shrub, small-mid tree, mid-large tree, and large tree, respectively. The selection of the height strata was made empirically by referring to in-situ tree height measurements. We identified the height stratum of tree structure loss from the changes in LiDAR point density for each 30 m pixel: first, we calculated the ratios of LiDAR points in each height strata according to their aboveground height (z values); then we recorded the height stratum where the LiDAR point ratio experienced the largest reduction from pre- to post-treatment; finally, we labelled the treatment height level as the recorded height stratum for each pixel in the treated boundary.

3. Results

3.1. AGB and vegetation indices maps

The plot-level AGB estimation from LiDAR-derived height metrics showed strong correlations with field measurements in both pre- and post-treatment datasets (Fig. 2). The correlation coefficients were similar between the two datasets, 0.784 for pre-treatment and 0.783 for post-treatment. The root-mean-squared-error between simulated and measured plot total AGB were 4.881 Mg and 4.822 Mg for pre- and post-treatment, respectively. Most of the LiDAR simulated AGB matched well with field measurements, except for one plot where the LiDAR-based total AGB was 10 Mg lower than the field measurement in the pre-treatment data.

The final LiDAR-derived AGB maps presented a wide range of biomass varying from 0 Mg/ha to 1500 Mg/ha in the study area (Fig. 3). Trees with large AGB values mainly clustered in the southwest (500–1500 Mg/ha), whereas the northeast of the study area had smaller AGB values (0–200 Mg/ha) (Fig. 3a and b). Within the USFS proposed treatment boundaries, the majority of the area (65.11%) observed AGB reduction after treatment (Fig. 3c). The mean AGB values within the treatment boundary decreased from 265.64 Mg/ha to 220.36 Mg/ha, and the standard deviation of AGB values also dropped from 183.53 Mg/ha to 150.82 Mg/ha. The AGB values in the remainder of the proposed treated area (approximately 35%) remained unchanged or slightly increased during the five-year period. Some areas outside the treatment boundary (21.86%) also experienced obvious AGB decreases, potentially up to 100 Mg/ha during the past five years.

The NDVI maps and their changes show similar patterns to AGB maps (Fig. 3), with higher values in the southwest and lower values in the northeast. A significant drop in NDVI values can be observed within the proposed treatment boundary, with the mean NDVI values changed from 0.76 in the pre-treatment to 0.59 after treatment. The mean NDVI value outside the treatment boundary indicated a marginal decrease in AGB, which was ten times smaller than that inside the boundary. Overall, the spatial extent and distribution of NDVI reduction matched well with AGB changes. However, the NDVI change map failed to capture some fine-scale isolated changes in forest biomass which were obvious from the AGB change map.

The histograms of NDVI and AGB show different shapes, both in the original values (Fig. 4a and c), and in the change values over the treated areas (Fig. 4b and d). The AGB histograms over the whole area (Fig. 4a) were right-skewed and peaked at low values (approximately 200 Mg/ha), whereas the NDVI histograms (Fig. 4c) peaked at large values (approximately at 0.8) for both pre- and post-treatment datasets. Within the treatment boundary, the histogram of AGB changes had a single peak (around 0 Mg/ha) and a long left-tail (Fig. 4b), but the histogram of NDVI changes presented double-peak at −0.2 and 0, respectively.

3.2. Overall correlations between changes in AGB and vegetation indices

The correlations between changes in two LiDAR-derived forest structural metrics (AGB and canopy cover) and Landsat-derived vegetation indices were significantly positive among all the four indices (NDVI, NDWI, TCA, and NBR) (Fig. 5). Pearson's correlation coefficients (R) among the four vegetation indices were consistent over the whole area, varying from 0.42 to 0.43 in AGB and from 0.7 to 0.73 in canopy cover. Vegetation indices were more sensitive to structural changes in canopy cover than AGB, as R was 70% higher in canopy cover than in AGB on average. The four vegetation indices demonstrated strong linear correlations, particularly between NDWI and NBR (R = 0.97), and between NDVI and TCA (R = 0.97).

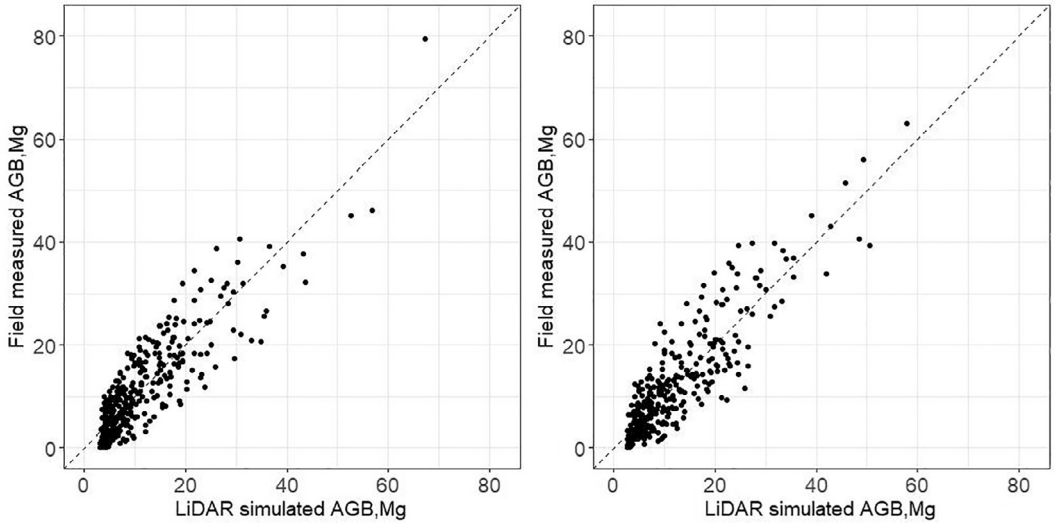

Fig. 2. Scatter plots of total AGB from LiDAR data against field measurements at plot-level for both pre-treatment (left) and post-treatment (right) datasets. The dashed line indicates the 1:1 line.

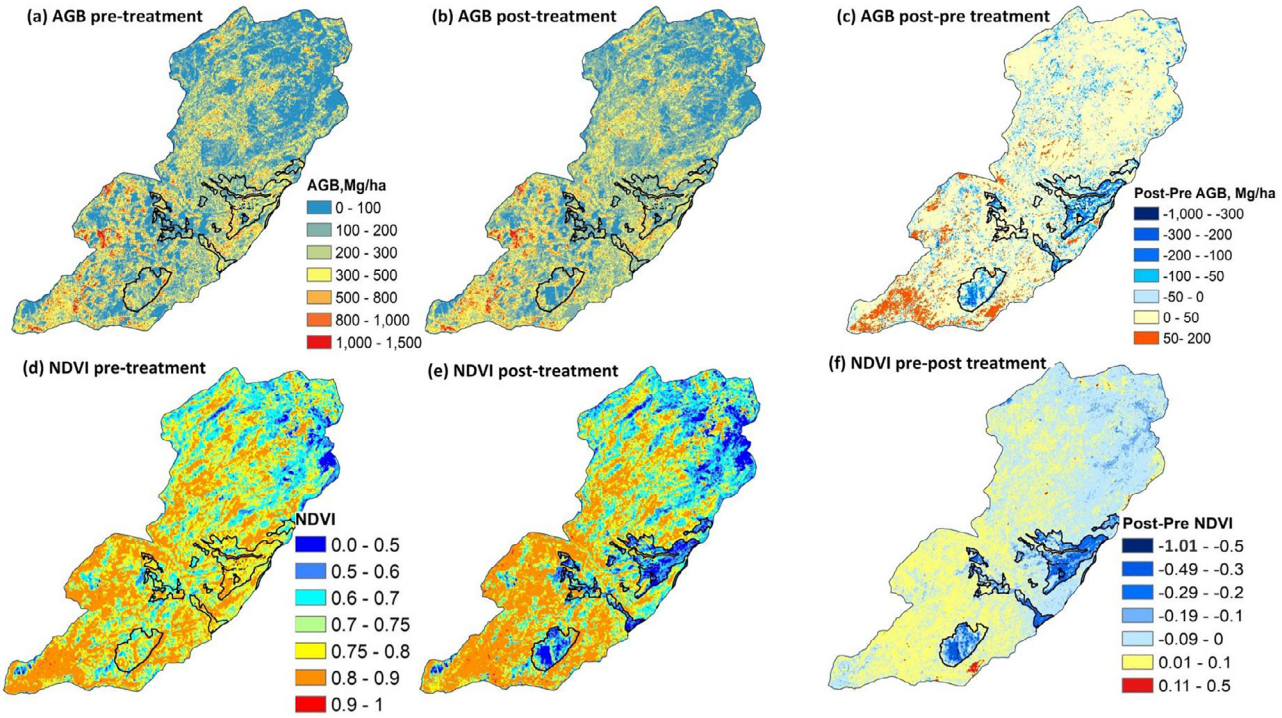

Fig. 3. LiDAR-derived AGB maps for: (a) pre-treatment (2008); (b) post-treatment (2013); and (c) the difference between post- and pre-treatment. Landsat-derived NDVI maps for: (d) pre-treatment (2008); (e) post-treatment (2013); and (f the difference between post- and pre-treatment.

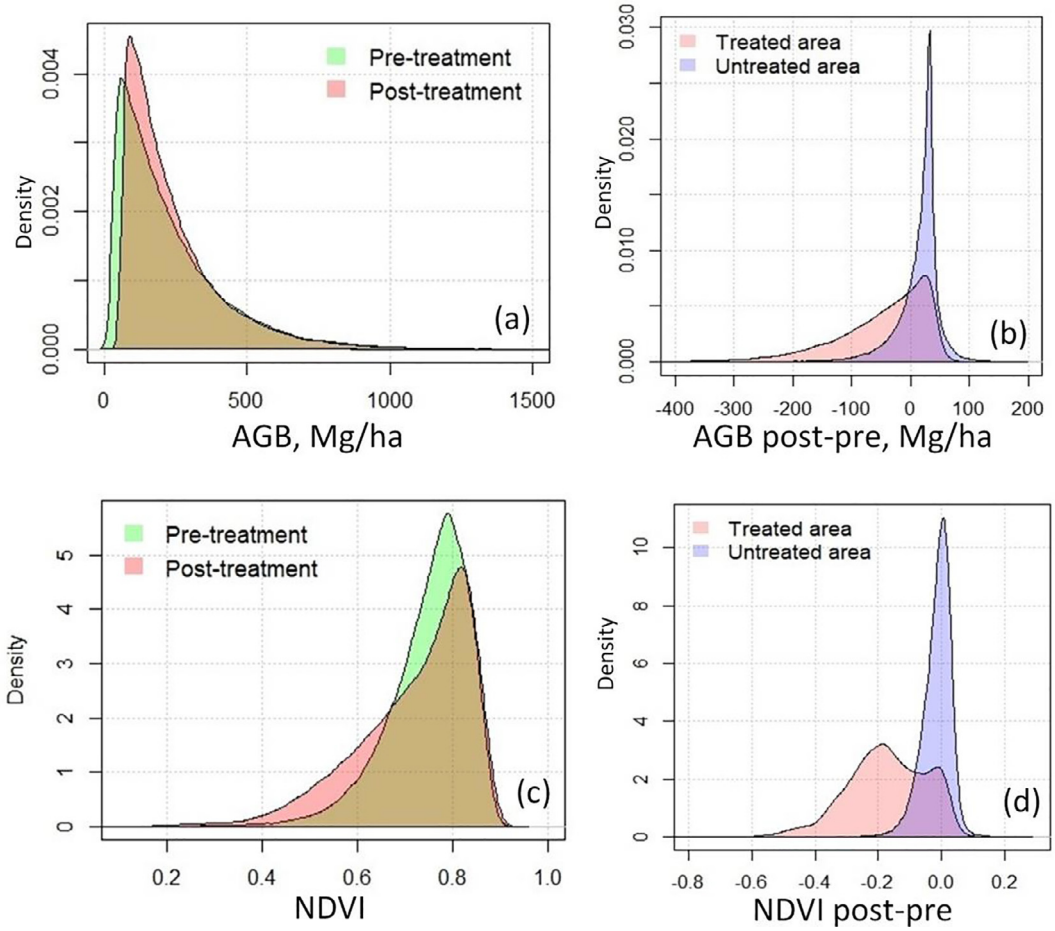

Fig. 4. Histograms of AGB values: (a) over the study area from pre-and post-treatment; and (b) AGB changes within and outside the treatment boundary. Histograms of NDVI values: (c) over the study area from pre-and post-treatment; and (d) NDVI changes within and outside the treatment boundary.

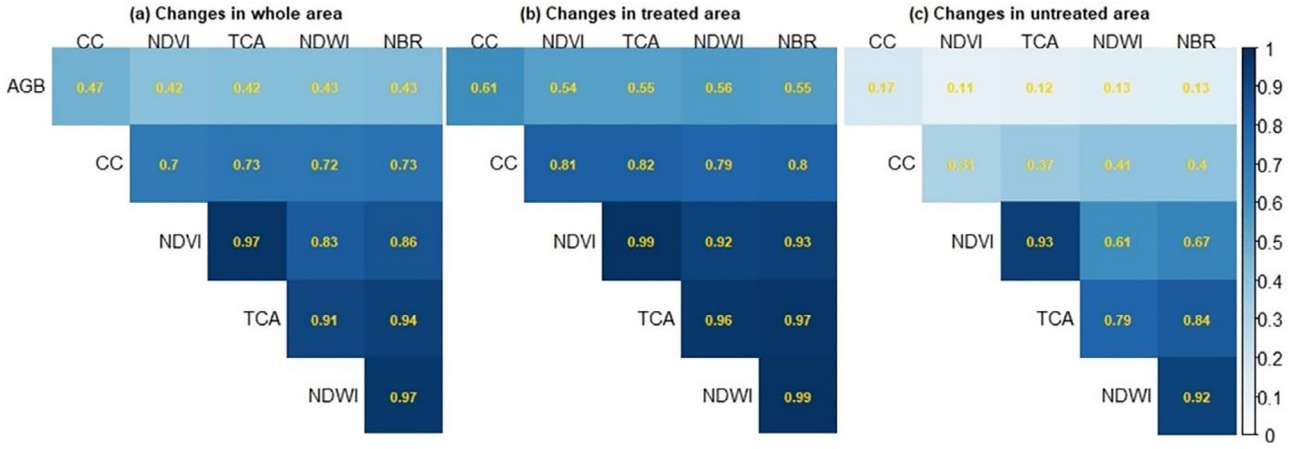

Fig. 5. Correlation matrices between changes in two LiDAR-derived structural parameters (AGB and canopy cover (CC)) and four vegetation indices (NDVI, TAC, NDWI, NBR) for (a) the entire study area; (b) within the treatment boundary; and (c) outside the treatment boundary (untreated area).

The correlation matrixes derived from inside and outside the treatment boundary were generally similar to that over the whole area. Changes in vegetation indices are more sensitive to canopy cover than AGB. However, the correlations were the strongest within the treatment boundary (Fig. 5b), followed by the whole area (Fig. 5a), and were the weakest outside the treatment boundary (Fig. 5c). On average, the correlations between vegetation indices and canopy cover within the treatment boundary were 100% higher than that outside the treatment boundary. The correlation coefficient between NDVI and AGB was 0.54 inside the treatment boundary, but was as low as 0.11 outside the boundary, although both correlations were significant at 99.9% level. Since the four vegetation indices demonstrated similar responses to forest structural changes, we chose the most widely used vegetation index, NDVI, to further analyze its sensitives to AGB changes in different scenarios.

3.3. Correlations among various forest densities and treatment levels

Changes in NDVI can partly predict the spatial variations in the AGB change map, and the strength of the prediction varied substantially among forests with different biomass densities before treatments (Fig. 6). Over the whole area, the coefficient of determination (R^2) between NDVI changes and AGB changes increased from low-biomass forest ($R^2 = 0.21$ at 0–100 Mg/ha) to medium-biomass forest ($R^2 = 0.49$, 200–300 Mg/ha), and the R^2 declined between forests with 300–400 Mg/ha and forests with 700–2000 Mg/ha. A similar trend was observed among AGB groups in the treated area, but the highest R^2 was achieved in a slightly large AGB group ($R^2 = 0.68$ at 300–400 Mg/ha) compared to the whole area. More significantly, the NDVI changes in the treated area demonstrated stronger prediction of AGB changes: the R^2 in the treated area was 81% higher than the whole area, and 500% higher than the untreated area on average among all pre-treatment AGB groups. Even in the largest pre-treatment AGB group, the R^2 was as high as 0.37 inside the treated area. Outside the treated area, the sensitivity of NDVI changes to AGB changes were low in general ($R^2 < 0.2$), and the correlations were lower in forests with largest biomass. It should be noted that the area of forests varied among AGB groups, as well as between treated/untreated areas: the low-to-mid pre-treatment AGB groups (0–400 Mg/ha) occupied larger proportions of the study area than the large groups (400–2000 Mg/ha).

A further examination of the capability of NDVI to represent AGB and canopy cover over forests of different densities for both pre- and

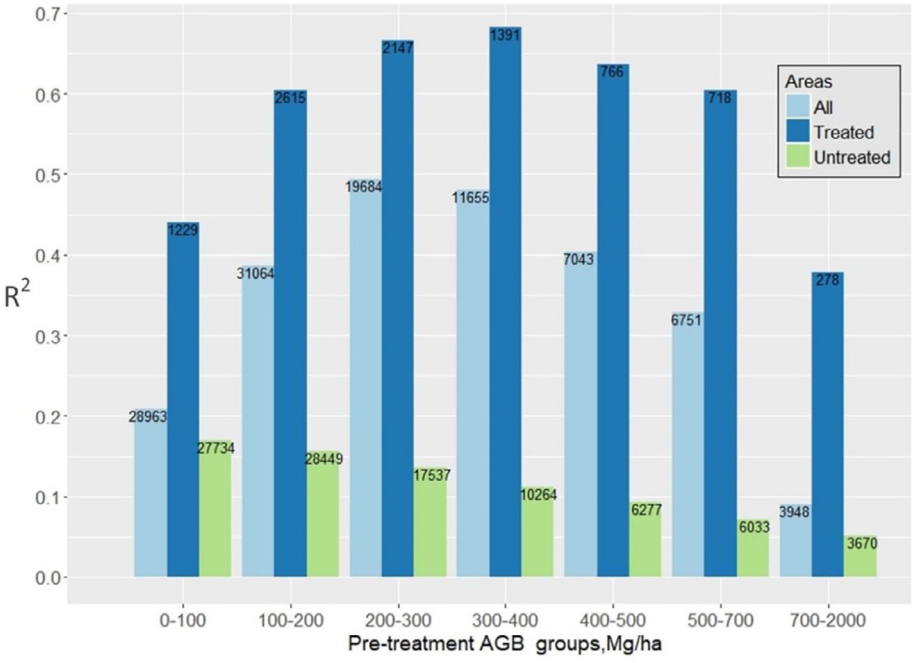

Fig. 6. Correlations between changes in NDVI and AGB grouping by pre-treatment AGB values in whole area (light blue), inside the treatment boundary (dark blue) and outside the treatment boundary (green). The numbers on the bar indicate the Landsat pixels in each group. (For interpretation of the references to colour in this figure legend, the reader is referred to the web version of this article.)

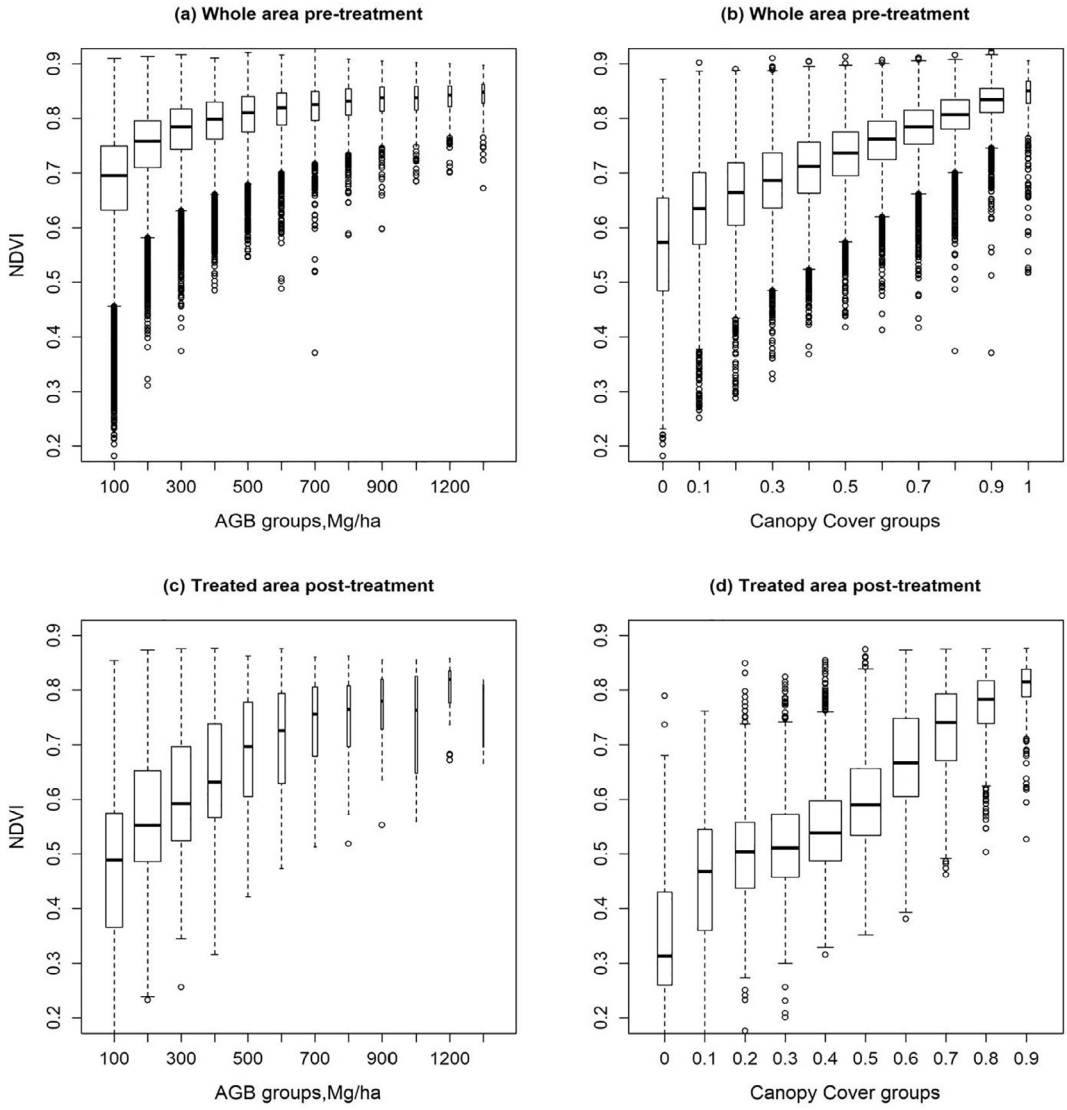

Fig. 7. Boxplots comparing: (a) NDVI and grouped AGB over the entire study area pre-treatment; (b) NDVI and grouped canopy cover over the entire study area pre-treatment; and (c) NDVI and grouped AGB for the treated area post-treatment; (d) NDVI and grouped canopy cover for the treated area post-treatment. The width of box is proportional to the number of observations in each group.

post-treatment are presented in Fig. 7. Before the treatment, NDVI was barely sensitive to AGB change in the densest forests (i.e. pre-treatment AGB greater than 600 Mg/ha in Fig. 7a), which indicated the saturation effect of NDVI when relating to AGB in dense forests. The NDVI saturation effect in NDVI was less severe within the treated area, particularly when relating post-treatment NDVI to AGB values (Fig. 7c). In contrast, the saturation effect when relating NDVI to canopy cover was marginal until the forest canopy cover approached full coverage (100%) for all areas from both pre- and post-treatment datasets (Fig. 7b and d).

The effectiveness of NDVI in quantifying fuel treatments was also influenced by the height of the treatments. In this study, as there were no detailed in-situ records on how forest treatments were conducted, or what sizes of trees were removed, we used the relative changes in LiDAR point density to classify treatments into different height strata. In the highest stratum, most of the tall trees (height > 20 m) were removed; whereas in the lower ones, treatments were mainly focused on small trees, shrubs, or understory fuels. An example from two typical sites is shown in Fig. 8 depicting the difference between clear cutting of large trees in > 20 m height class (Fig. 8a and b) and understory fuel removing in the 5–10 m height class (Fig. 8c and d) is apparent from the LiDAR point clouds. A correlation analysis between changes in NDVI and AGB among the four treatment classes indicated that the strongest correlation ($R^2 = 0.43$) was observed in treated areas where the majority of LiDAR point density reduction occurred in the highest stratum (height > 20 m). The R^2 dropped dramatically when the treatment occurred in the lower canopy or closer to the ground surface (Fig. 9). Overall, NDVI changes can better quantify AGB decrease induced by the removal of larger trees rather than smaller trees or understory treatments.

The sensitivity of NDVI to forest fuel treatments was influenced by the combined effect of both pre-treatment forest density and treatment intensity. To illustrate this combined effect, we further categorized the decreased AGB pixels into four classes with similar pixel numbers but different pre-treatment biomass densities and examined how NDVI responded to various amounts of AGB decrease among the four groups (Fig. 10). Results indicated that in the low pre-treatment AGB group (0–250 Mg/ha) a slight reduction in AGB (40 Mg/ha) could lead to substantial decreased in NDVI (0.2 on average), whereas in the high pre-treatment AGB groups (400–500 Mg/ha and 500–1500 Mg/ha), the mean NDVI changes did not respond to AGB disturbances until the reduction exceeded 80 Mg/ha and 100 Mg/ha, respectively. Overall,

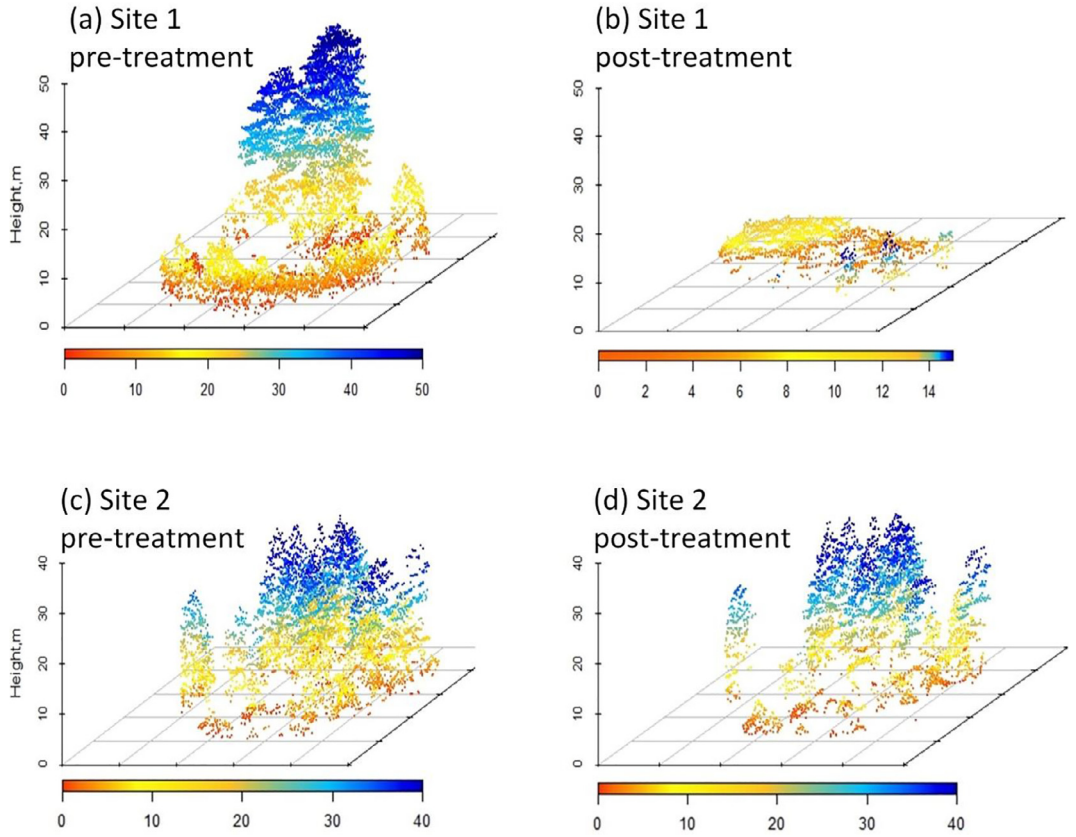

Fig. 8. Examples of the changes in LiDAR point clouds after fuel treatments conducted in high canopy levels (Site 1 (a) and (b)) and low canopy levels (Site 2 (c) and (d)).

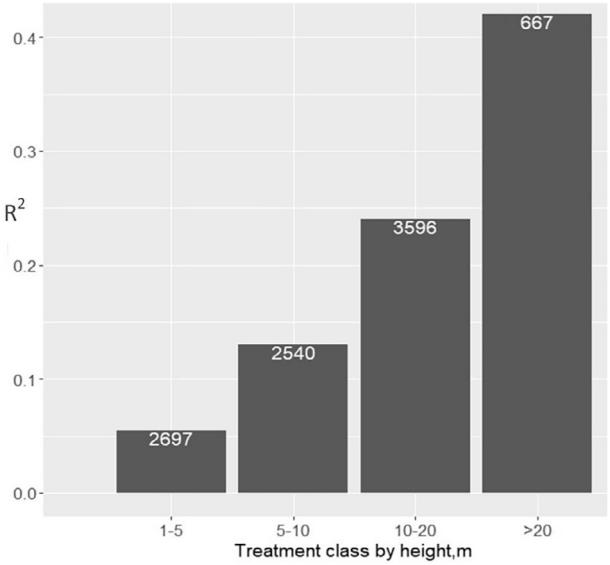

Fig. 9. Correlations between changes in NDVI and AGB grouping by treatments conducted at different height strata. The numbers on each bar indicate the Landsat pixels in each class.

the NDVI was barely sensitive to fuel treatments in extremely dense forests, but tented to be over-sensitive in sparse forests, even to mild treatments.

4. Discussion

4.1. Comparison between vegetation indices and forest structural changes

Four widely used Landsat-derived vegetation indices were evaluated regarding their effectiveness in quantifying treatment induced forest structural changes. We found the difference among them was marginal (< 10%); this suggests that the high collinearity among them (e.g. Fig. 5) was partly due to the fact that all indices were generated from the annual MVC surface reflectance data. MVC removed most of the seasonal changes in vegetation (Delbart et al., 2006), and consequently may also reduce the overall variations among the four vegetation indices. NDWI was designed to detect the water availability (Gao, 1996; Gu et al., 2007), whereas NBR was developed to indicate fire severity (Key and Benson, 2006; Miller and Thode, 2007). Their applications in monitoring forest biomass changes induced by treatments have been less common than NDVI because NDVI is a stronger indicator of forest greennes and biomass (Gamon et al., 1995; Tucker, 1979; Veraverbeke et al., 2012; Viedma et al., 1997). The TCA integrated information from six bands of Landsat data rather than two bands as the other three indices (Gómez et al., 2011). Due to the higher complexity in TCA calculation, the TCA-derived change does require more normalization from field measurements to enable comparisons among sites (Gómez et al., 2011), and thus may limit its applications in broad areas. Some other indices, such as the enhanced vegetation index and reduced simple ratio have also been used to monitor forest changes (Chen et al., 2005; Jin and Sader, 2005), but less frequently in previous studies, and thus their performances were not evaluated in this study. Overall, NDVI has a longer history and broader usage in representing the forest greenness, biomass, and leaf area index, and thus is more pervasive in forest changes monitoring than the other indices (Gamon et al., 1995; Tucker, 1979; Veraverbeke et al., 2012; Viedma et al., 1997).

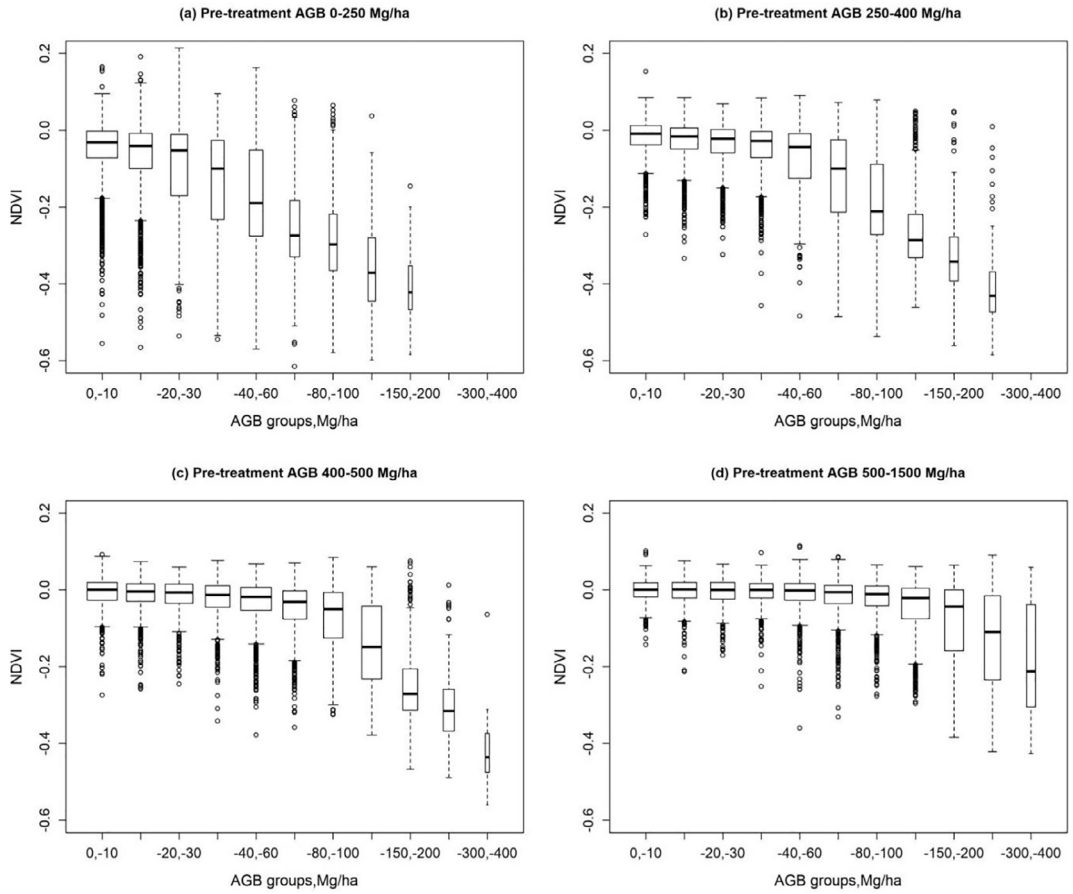

Fig. 10. Boxplots of NDVI changes in different AGB change groups. The four boxplots represent (a) pre-treatment AGB in small (0–250 Mg/ha); (b) small-mid (250–400 Mg/ha); (c) mid-large (400–500 Mg/ha); and (d) large (500–2000 Mg/ha) groups. The width of box is proportional to the number of observations in each group.

Our results indicated that all the vegetation indices showed higher correlations to changes in canopy cover than AGB (Fig. 5). Similar conclusions have been suggested in some previous studies (Gamon et al., 1995; Gao et al., 2000; Mutanga and Skidmore, 2004). Their less sensitivity to AGB is mainly because vegetation indices often fail to indicate the further increase of AGB in forests denser than a certain amount. This phenomenon has been described as the saturation effect of vegetation indices in a previous study (Mutanga and Skidmore, 2004). Gamon et al. (1995) found that the saturation effect in NDVI when relating it to AGB and other structural parameters could be influenced by many factors, including vegetation type, canopy senescence, soil background, and sensor and sun geometry. In this study, the saturation effect of NDVI was apparent in relation to AGB, particularly in the forests where pre-treatment AGB was larger than 600 Mg/ha (Fig. 7). In contrast, the saturation effect was marginal in relation to canopy cover even if the canopy cover approached 100% (Fig. 7). The stronger saturation effect in AGB might also be due to the larger uncertainty in AGB estimation comparing to canopy cover. Although one of the most accurate wall-to-wall AGB estimation methods was adopted in this study (e.g. regression based on LiDAR-metrics and plot-measured biomass), uncertainties could have been introduced from bias in field measurements, as well as the generation of the relationship between field-measured AGB and LiDAR metrics. The bias in AGB estimation could be up to 25%, according to a study conducted in the same location (Li et al., 2015). The canopy cover map, on the contrary, was generated directly from LiDAR data, and thus had less sources of uncertainties (Ma et al., 2017a).

In this study area, the NDVI saturation effect was less severe within the treated area after the fuel treatment (Fig. 8), mostly due to the decreased canopy density, and this also explained why the relationships between changes in NDVI and AGB in treated area were stronger than that over the whole area. Gamon et al. (1995) mentioned that satellite-derived vegetation indices, such as NDVI and simple ratio, were stronger indicators of green-biomass rather than total biomass. It is possible that the correlations between NDVI and green-AGB could be stronger than current NDVI and total-AGB relationships. However, due to the lack of explicit information on whether the sampled trees were dead or alive, with yellow, red or green leaves, it was difficult to distinguish green-AGB from total-AGB purely using LiDAR measurements.

4.2. Uncertainties related to forest densities

In this paper we analyzed the uncertainty by comparing responses of NDVI to AGB and canopy cover changes under different forest densities and treatment intensities. The uncertainty of using NDVI to quantify the forest biomass changes was smaller in the medium-biomass groups (200–300 Mg/ha and 300–400 Mg/ha) than the extremely low (0–100 Mg/ha) or high (700–2000 Mg/ha) pre-treatment AGB groups, as indicated by the variations in the correlations between changes in NDVI and AGB in different forest density groups (Fig. 6). The larger uncertainty can partly be explained by the over-sensitivity of NDVI to AGB disturbance in sparse forests, and its saturation effect in extremely dense forest. A minor AGB reduction in sparse forests can lead to substantial decrease in NDVI, whereas in extremely dense forests, NDVI might not be responsive even to a decent amount of biomass removal.

Vegetation indices from time series satellite imagery have been used to map forest treatments and evaluate their hydrological and ecological impacts through relating changes in vegetation indices to reductions in

basal area and/or biomass (DeVries et al., 2015; Huang et al., 2010; Masek et al., 2008). However, our results showed that the robustness of the relationships varied substantially by the pre-treatment forest densities. In the low AGB areas, a small reduction (< 30 Mg/ha) in biomass could result in decent amount of NDVI decrease (up to 0.4). The removal of some small trees in sparse forests may expose ground surface and even bare earth, and result in the sharp decrease of NDVI to extremely low values (close to 0). In contrast, the NDVI values in extremely dense forests may remain unchanged after fuel treatments because NDVI is saturated even after removing some large trees. Therefore, cautions should be paid to the over-sensitivity and saturation effects in Landsat-derived vegetation indices when using them to quantify forest biomass changes in either extremely sparse or dense forests. Due to the limited coverage of LiDAR and field measurement in this study, we only evaluated the Landsat-derived vegetation indices in a typical mixed-conifer dominated forest. Results drawn from this forest stand may be representative of Sierra Nevada mixed-conifer forests, but not necessarily applicable to other regions with different biomes and/or climates. More studies are needed to thoroughly evaluate the capabilities and limitations of Landsat-derived vegetation and clarify its uncertainties in biomass change quantification over large areas.

4.3. Uncertainties related to different treatments

Forest fuel treatments are a common management practice in Sierra Nevada forests for many reasons, including wildlife habitat protection, fire risk exclusion, and drought stress release (Knapp et al., 2013, 2017; Park et al., 2018; Battles et al., 2001; Stephens et al., 2009). Depending on the purposes, fuel treatments can be achieved in many ways. Some fuel treatments focused on the removal of overstory trees, particularly large trees (> 20 in. dbh), in order to reduce overstory canopy cover and increase sunlight exposure in understory. Increasing the forest heterogeneity both vertically and horizontally was critically important for wildlife habitation protection, because spatial variations are desirable for sustaining adequate food and biodiversity at different scales from forest stand to landscape (Franklin et al., 2002). For example, the spotted owl prefers forests with snags and large trees for prey and nesting (Stephens et al., 2016b; Tempel et al., 2014). In contrast, fire suppression often focuses on thinning the surface fuel, tree ladders, or small understory trees, because they are more likely to cause the spread of fires, whereas large trees (dbh > 20 in.) are less impacted in forest fires (Stephens et al., 2009). Responding to different forest management goals, treatments are often conducted using a range of equipment and methods, i.e. mechanical treatment, hand thinning, piling, and chain removing (Knapp et al., 2017). Their impacts on forest structures will vary accordingly, which could be challenging for treatment mapping and biomass change quantification at regional scales using remote sensing techniques.

In this study, we categorized fuel treatment levels by referencing to the changes in point density over various height strata (Fig. 10) because we lacked detailed documentation regarding treatment strategies. The LiDAR data may not fully delineate forest structure changes due to limitations in point density and laser penetration capability in extremely dense forests (Jakubowksi et al., 2013). However, by comparing the two LiDAR datasets, obtained using similar flight parameters and in the same season, we considered the comparison of the point clouds as an appropriate reference to categorize different treatment strategies. Forest stands that were treated at high strata by removing most of the tall and big trees were better quantified using vegetation indices, whereas the biomass reduction caused by understory thinning on small trees (< 10 m) or understory fuels was more difficult to quantify. Our results suggest that using Landsat-derived vegetation indices to monitor forest fuel treatments or to assess the impacts on forest structures is most reliable when the objectives were the removal of overstory trees. Landsat-derived vegetation indices can be used to detect some of the understory thinning or fuel reduction at certain levels, but the uncertainties can be huge when the major biomass reduction occurred lower than 10 m. Our study characterized treatments merely based on the changes in LiDAR-point density, more studies with detailed documentation of treatment methods are needed to fully illustrate how well Landsat-derived vegetation indices can quantify biomass changes.

5. Conclusions

Landsat-derived vegetation indices have been widely used to map and monitor forest ecosystem dynamics over long-term periods from regional to global scales. Our study evaluated their uncertainties in indicating the forest biomass loss induced by forest fuel treatments using wall-to-wall validation data derived from LiDAR and field measurements. The four widely used vegetation indices, NDVI, NDWI, NBR, and TCA, performed equally well in characterizing canopy cover loss due to forest fuel treatments, but their capabilities in predicting variations in aboveground biomass loss were less satisfactory. Focusing on the most widely used vegetation index, NDVI, we found that uncertainties mainly resulted from the saturation and over-sensitivity of NDVI in representing the biomass changes at extremely dense or sparse forests, respectively. In conclusion, vegetation indices like NDVI are more suitable for quantifying biomass changes in forests with mid-density ranges rather than extremely sparse or dense forests. The accuracy of NDVI in predicting aboveground biomass changes were also influenced by the treatment types, which decreased sequentially as the treatments implemented from the over story to the ground surface. Overall, vegetation indices from satellite imagery can detect and map changes in canopy cover and land cover types induced by treatments and other disturbances. However, when the objectives are to quantify forest dynamics in carbon stock or water usage, researchers and managers should pay more attention to the potential bias in applying vegetation indices over extremely dense or sparse forests. Moreover, forest fuel treatments, such as surface fuel clearing and understory thinning, are difficult to monitor precisely from Landsat-derived vegetation indices alone.

Acknowledgments

This study was funded by the National Science Foundation (DBI 1356077). We acknowledge the contribution of the Sierra Nevada Adaptive Management Project, an interagency project supported by the USDA Forest Service Region 5, USDA Forest Service Pacific Southwest Research Station, US Fish and Wildlife Service, California Department of Water Resources, California Department of Fish and Wildlife, California Department of Forestry and Fire Protection, and the Sierra Nevada Conservancy. We also thank Joseph Rungee from University of California, Merced, for his help in grammar checking and editing.

References

Agee, J.K., Skinner, C.N., 2005. Basic principles of forest fuel reduction treatments. For. Ecol. Manage. 211, 83–96.
Asner, G.P., Mascaro, J., 2014. Mapping tropical forest carbon: calibrating plot estimates to a simple LiDAR metric. Remote Sens. Environ. 140, 614–624.
Bales, R.C., Battles, J.J., Chen, Y., Conklin, M.H., Holst, E., O'Hara, K.L., Saksa, P., Stewart, W., 2011. Forests and water in the Sierra Nevada: Sierra Nevada watershed ecosystem enhancement project. Sierra Nevada Research Institute report.
Battles, J.J., Shlisky, A.J., Barrett, R.H., Heald, R.C., Allen-Diaz, B.H., 2001. The effects of forest management on plant species diversity in a Sierran conifer forest. For. Ecol. Manage. 146, 211–222.
Blanchard, S.D., Jakubowski, M.K., Kelly, M., 2011. Object-based image analysis of downed logs in disturbed forested landscapes using lidar. Remote Sens. 3, 2420–2439.
Chen, X., Vierling, L., Deering, D., 2005. A simple and effective radiometric correction method to improve landscape change detection across sensors and across time. Remote Sens. Environ. 98, 63–79.
Cohen, W.B., Yang, Z., Stehman, S.V., Schroeder, T.A., Bell, D.M., Masek, J.G., Huang, C., Meigs, G.W., 2016. Forest disturbance across the conterminous United States from 1985–2012: the emerging dominance of forest decline. For. Ecol. Manage. 360,

242–252.
Collins, B.M., Everett, R.G., Stephens, S.L., 2011a. Impacts of fire exclusion and recent managed fire on forest structure in old growth Sierra Nevada mixed-conifer forests. Ecosphere 2, 1–14.
Collins, B.M., Lydersen, J.M., Everett, R.G., Fry, D.L., Stephens, S.L., 2015. Novel characterization of landscape-level variability in historical vegetation structure. Ecol. Appl. 25, 1167–1174.
Collins, B.M., Stephens, S.L., Roller, G.B., Battles, J.J., 2011b. Simulating fire and forest dynamics for a landscape fuel treatment project in the Sierra Nevada. For. Sci. 57, 77–88.
Coops, N.C., Hilker, T., Wulder, M.A., St-Onge, B., Newnham, G., Siggins, A., Trofymow, J.T., 2007. Estimating canopy structure of Douglas-fir forest stands from discrete-return LiDAR. Trees 21, 295–310.
Crist, E.P., 1985. A TM Tasseled Cap equivalent transformation for reflectance factor data. Remote Sens. Environ. 17, 301–306.
Crist, E.P., Cicone, R.C., 1984. A physically-based transformation of thematic mapper data—the TM tasseled cap. IEEE Trans. Geosci. Remote Sens. GE-22, 256–263.
Dalponte, M., Frizzera, L., Ørka, H.O., Gobakken, T., Næsset, E., Gianelle, D., 2018. Predicting stem diameters and aboveground biomass of individual trees using remote sensing data. Ecol. Ind. 85, 367–376.
Delbart, N., Le Toan, T., Kergoat, L., Fedotova, V., 2006. Remote sensing of spring phenology in boreal regions: a free of snow-effect method using NOAA-AVHRR and SPOT-VGT data (1982–2004). Remote Sens. Environ. 101, 52–62.
DeVries, B., Verbesselt, J., Kooistra, L., Herold, M., 2015. Robust monitoring of small-scale forest disturbances in a tropical montane forest using Landsat time series. Remote Sens. Environ. 161, 107–121.
Franklin, J.F., Spies, T.A., Pelt, R.V., Carey, A.B., Thornburgh, D.A., Berg, D.R., Lindenmayer, D.B., Harmon, M.E., Keeton, W.S., Shaw, D.C., Bible, K., Chen, J., 2002. Disturbances and structural development of natural forest ecosystems with silvicultural implications, using Douglas-fir forests as an example. For. Ecol. Manage. 155, 399–423.
Gamon, J.A., Field, C.B., Goulden, M.L., Griffin, K.L., Hartley, A.E., Joel, G., Penuelas, J., Valentini, R., 1995. Relationships between NDVI, canopy structure, and photosynthesis in three californian vegetation types. Ecol. Appl. 5, 28–41.
Gao, B.-C., 1996. NDWI—a normalized difference water index for remote sensing of vegetation liquid water from space. Remote Sens. Environ. 58, 257–266.
Gao, X., Huete, A.R., Ni, W., Miura, T., 2000. Optical-biophysical relationships of vegetation spectra without background contamination. Remote Sens. Environ. 74, 609–620.
Gleason, C.J., Im, J., 2012. Forest biomass estimation from airborne LiDAR data using machine learning approaches. Remote Sens. Environ. 125, 80–91.
Gómez, C., White, J.C., Wulder, M.A., 2011. Characterizing the state and processes of change in a dynamic forest environment using hierarchical spatio-temporal segmentation. Remote Sens. Environ. 115, 1665–1679.
Gorelick, N., Hancher, M., Dixon, M., Ilyushchenko, S., Thau, D., Moore, R., 2017. Google earth engine: planetary-scale geospatial analysis for everyone. Remote Sens. Environ. 202, 18–27.
Gu, Y., Brown, J.F., Verdin, J.P., Wardlow, B., 2007. A five-year analysis of MODIS NDVI and NDWI for grassland drought assessment over the central Great Plains of the United States. Geophys. Res. Lett. 34.
Guo, Q., Li, W., Yu, H., Alvarez, O., 2010. Effects of topographic variability and lidar sampling density on several DEM interpolation methods. Photogramm. Eng. Remote Sens. 76, 701–712.
Hansen, M.C., Potapov, P.V., Moore, R., Hancher, M., Turubanova, S., Tyukavina, A., Thau, D., Stehman, S., Goetz, S., Loveland, T., 2013. High-resolution global maps of 21st-century forest cover change. Science 342, 850–853.
Holben, B.N., 1986. Characteristics of maximum-value composite images from temporal AVHRR data. Int. J. Remote Sens. 7, 1417–1434.
Hopkinson, P., Huber, A., Saah, D.S., Battles, J.J., 2017. A word to the wise: advice for scientists engaged in collaborative adaptive management. Environ. Manage. 59, 752–761.
Huang, C., Goward, S.N., Masek, J.G., Thomas, N., Zhu, Z., Vogelmann, J.E., 2010. An automated approach for reconstructing recent forest disturbance history using dense Landsat time series stacks. Remote Sens. Environ. 114, 183–198.
Huang, C., Goward, S.N., Schleeweis, K., Thomas, N., Masek, J.G., Zhu, Z., 2009. Dynamics of national forests assessed using the Landsat record: case studies in eastern United States. Remote Sens. Environ. 113, 1430–1442.
Huang, C., Wylie, B., Yang, L., Homer, C., Zylstra, G., 2002. Derivation of a tasselled cap transformation based on Landsat 7 at-satellite reflectance. Int. J. Remote Sens. 23, 1741–1748.
Jakubowksi, M.K., Guo, Q., Collins, B., Stephens, S., Kelly, M., 2013. Predicting surface fuel models and fuel metrics using Lidar and CIR imagery in a dense, mountainous forest. Photogramm. Eng. Remote Sens. 79, 37–49.
Jenkins, J.C., Chojnacky, D.C., Heath, L.S., Birdsey, R.A., 2003. National-scale biomass estimators for United States tree species. For. Sci. 49, 12–35.
Jin, S., Sader, S.A., 2005. MODIS time-series imagery for forest disturbance detection and quantification of patch size effects. Remote Sens. Environ. 99, 462–470.
Kelly, M., Di Tommaso, S., 2015. Mapping forests with Lidar provides flexible, accurate data with many uses. Calif. Agric. 69, 14–20.
Kelly, M., Su, Y., Di Tommaso, S., Fry, D.L., Collins, B.M., Stephens, S.L., Guo, Q., 2017. Impact of error in lidar-derived canopy height and canopy base height on modeled wildfire behavior in the Sierra Nevada, California, USA. Remote Sens. 10, 10.
Kennedy, R.E., Yang, Z., Cohen, W.B., 2010. Detecting trends in forest disturbance and recovery using yearly Landsat time series: 1. LandTrendr — temporal segmentation algorithms. Remote Sens. Environ. 114, 2897–2910.
Kerr, G., Haufe, J., 2011. Thinning Practice: A Silvicultural Guide. Forestry Commission, Edinburgh.
Key, C., Benson, N., 2006. Landscape assessment: ground measure of severity, the Composite Burn Index. In: Lutes, D.C. (Ed.), FIREMON: Fire Effects Monitoring and Inventory System. USDA Forest Service, Rocky Mountain Research Station, Fort Collins, Colorado, USA, pp. LA8–LA15.
Knapp, E.E., Lydersen, J.M., North, M.P., Collins, B.M., 2017. Efficacy of variable density thinning and prescribed fire for restoring forest heterogeneity to mixed-conifer forest in the central Sierra Nevada, CA. For. Ecol. Manage. 406, 228–241.
Knapp, E.E., Skinner, C.N., North, M.P., Estes, B.L., 2013. Long-term overstory and understory change following logging and fire exclusion in a Sierra Nevada mixed-conifer forest. For. Ecol. Manage. 310, 903–914.
Korhonen, L., Korpela, I., Heiskanen, J., Maltamo, M., 2011. Airborne discrete-return LIDAR data in the estimation of vertical canopy cover, angular canopy closure and leaf area index. Remote Sens. Environ. 115, 1065–1080.
Korhonen, L., Morsdorf, F., 2014. Estimation of canopy cover, gap fraction and leaf area index with airborne laser scanning. In: Forestry Applications of Airborne Laser Scanning. Springer, pp. 397–417.
Kramer, H.A., Collins, B.M., Gallagher, C.V., Keane, J., Stephens, S.L., Kelly, M., 2016. Accessible light detection and ranging: estimating large tree density for habitat identification. Ecosphere 7.
Kramer, H.A., Collins, B.M., Kelly, M., Stephens, S.L., 2014. Quantifying ladder fuels: a new approach using LiDAR. Forests 5, 1432–1453.
Li, L., Guo, Q., Tao, S., Kelly, M., Xu, G., 2015. Lidar with multi-temporal MODIS provide a means to upscale predictions of forest biomass. ISPRS J. Photogramm. Remote Sens. 102, 198–208.
Lim, K.S., Treitz, P.M., 2004. Estimation of above ground forest biomass from airborne discrete return laser scanner data using canopy-based quantile estimators. Scand. J. For. Res. 19, 558–570.
Luo, S., Wang, C., Xi, X., Pan, F., Peng, D., Zou, J., Nie, S., Qin, H., 2017. Fusion of airborne LiDAR data and hyperspectral imagery for aboveground and belowground forest biomass estimation. Ecol. Ind. 73, 378–387.
Ma, Q., Su, Y., Guo, Q., 2017a. Comparison of canopy cover estimations from airborne LiDAR, aerial imagery, and satellite imagery. IEEE J. Sel. Top. Appl. Earth Obs. Remote Sens.
Ma, Q., Su, Y., Tao, S., Guo, Q., 2017b. Quantifying individual tree growth and tree competition using bi-temporal airborne laser scanning data: a case study in the Sierra Nevada Mountains, California. Int. J. Digital Earth 1–19.
Magnussen, S., Næsset, E., Gobakken, T., 2015. LiDAR-supported estimation of change in forest biomass with time-invariant regression models. Can. J. For. Res. 45, 1514–1523.
Masek, J.G., Huang, C., Wolfe, R., Cohen, W., Hall, F., Kutler, J., Nelson, P., 2008. North American forest disturbance mapped from a decadal Landsat record. Remote Sens. Environ. 112, 2914–2926.
McCarley, T.R., Kolden, C.A., Vaillant, N.M., Hudak, A.T., Smith, A.M., Wing, B.M., Kellogg, B.S., Kreitler, J., 2017. Multi-temporal LiDAR and Landsat quantification of fire-induced changes to forest structure. Remote Sens. Environ. 191, 419–432.
Menning, K.M., Stephens, S.L., 2007. Fire climbing in the forest: a semiqualitative, semiquantitative approach to assessing ladder fuel hazards. West. J. Appl. For. 22, 88–93.
Miller, J.D., Thode, A.E., 2007. Quantifying burn severity in a heterogeneous landscape with a relative version of the delta Normalized Burn Ratio (dNBR). Remote Sens. Environ. 109, 66–80.
Mitchell, S.R., Harmon, M.E., O'connell, K.E., 2009. Forest fuel reduction alters fire severity and long-term carbon storage in three Pacific Northwest ecosystems. Ecol. Appl. 19, 643–655.
Mutanga, O., Skidmore, A.K., 2004. Narrow band vegetation indices overcome the saturation problem in biomass estimation. Int. J. Remote Sens. 25, 3999–4014.
Næsset, E., 1997. Determination of mean tree height of forest stands using airborne laser scanner data. ISPRS J Photogramm Remote Sens. 52.
Næsset, E., Bjerknes, K.O., 2001. Estimating tree heights and number of stems in young forest stands using airborne laser scanner data. Remote Sens. Environ. 78.
Næsset, E., Økland, T., 2002. Estimating tree height and tree crown properties using airborne scanning laser in a boreal nature reserve. Remote Sens. Environ. 79, 105–115.
Ni-Meister, W., Lee, S., Strahler, A.H., Woodcock, C.E., Schaaf, C., Yao, T., Ranson, K.J., Sun, G., Blair, J.B., 2010. Assessing general relationships between aboveground biomass and vegetation structure parameters for improved carbon estimate from lidar remote sensing. J. Geophys. Res. Biogeosci. 115.
Nilsson, M., 1996. Estimation of tree heights and stand volume using an airborne lidar system. Remote Sens. Environ. 56, 1–7.
Park, J., Kim, T., Moon, M., Cho, S., Ryu, D., Seok Kim, H., 2018. Effects of thinning intensities on tree water use, growth, and resultant water use efficiency of 50-year-old Pinus koraiensis forest over four years. For. Ecol. Manage. 408, 121–128.
Parsons, D.J., DeBenedetti, S.H., 1979. Impact of fire suppression on a mixed-conifer forest. For. Ecol. Manage. 2, 21–33.
Popescu, S.C., Zhao, K., 2008. A voxel-based lidar method for estimating crown base height for deciduous and pine trees. Remote Sens. Environ. 112, 767–781.
Saksa, P.C., Conklin, M.H., Battles, J.J., Tague, C.L., Bales, R.C., 2017. Forest thinning impacts on the water balance of Sierra Nevada mixed-conifer headwater basins. Water Resour. Res. 53, 5364–5381.
Schroeder, T.A., Healey, S.P., Moisen, G.G., Frescino, T.S., Cohen, W.B., Huang, C., Kennedy, R.E., Yang, Z., 2014. Improving estimates of forest disturbance by combining observations from Landsat time series with U.S. Forest Service Forest Inventory and Analysis data. Remote Sens. Environ. 154, 61–73.
Schroeder, T.A., Schleeweis, K.G., Moisen, G.G., Toney, C., Cohen, W.B., Freeman, E.A., Yang, Z., Huang, C., 2017. Testing a Landsat-based approach for mapping disturbance

causality in US forests. Remote Sens. Environ. 195, 230–243.
Schroeder, T.A., Wulder, M.A., Healey, S.P., Moisen, G.G., 2011. Mapping wildfire and clearcut harvest disturbances in boreal forests with Landsat time series data. Remote Sens. Environ. 115, 1421–1433.
Stephens, S.L., Collins, B.M., Biber, E., Fulé, P.Z., 2016a. US federal fire and forest policy: emphasizing resilience in dry forests. Ecosphere 7.
Stephens, S.L., Collins, B.M., Fettig, C.J., Finney, M.A., Hoffman, C.M., Knapp, E.E., North, M.P., Safford, H., Wayman, R.B., 2018. Drought, tree mortality, and wildfire in forests adapted to frequent fire. Bioscience.
Stephens, S.L., Miller, J.D., Collins, B.M., North, M.P., Keane, J.J., Roberts, S.L., 2016b. Wildfire impacts on California spotted owl nesting habitat in the Sierra Nevada. Ecosphere 7.
Stephens, S.L., Moghaddas, J.J., Edminster, C., Fiedler, C.E., Haase, S., Harrington, M., Keeley, J.E., Knapp, E.E., McIver, J.D., Metlen, K., 2009. Fire treatment effects on vegetation structure, fuels, and potential fire severity in western US forests. Ecol. Appl. 19, 305–320.
Su, Y., Bales, R.C., Ma, Q., Nydick, K., Ray, R.L., Li, W., Guo, Q., 2017. Emerging stress and relative resiliency of giant sequoia groves experiencing multiyear dry periods in a warming climate. J. Geophys. Res. Biogeosci. 122, 3063–3075.
Su, Y., Guo, Q., Collins, B.M., Fry, D.L., Hu, T., Kelly, M., 2016a. Forest fuel treatment detection using multi-temporal airborne lidar data and high-resolution aerial imagery: a case study in the Sierra Nevada Mountains, California. Int. J. Remote Sens. 37, 3322–3345.
Su, Y., Guo, Q., Xue, B., Hu, T., Alvarez, O., Tao, S., Fang, J., 2016b. Spatial distribution of forest aboveground biomass in China: estimation through combination of spaceborne lidar, optical imagery, and forest inventory data. Remote Sens. Environ. 173, 187–199.
Sulla-Menashe, D., Friedl, M.A., Woodcock, C.E., 2016. Sources of bias and variability in long-term Landsat time series over Canadian boreal forests. Remote Sens. Environ. 177, 206–219.
Tao, S., Guo, Q., Li, L., Xue, B., Kelly, M., Li, W., Xu, G., Su, Y., 2014. Airborne Lidar-derived volume metrics for aboveground biomass estimation: a comparative assessment for conifer stands. Agric. For. Meteorol. 198, 24–32.
Tempel, D.J., Gutiérrez, R., Battles, J.J., Fry, D.L., Su, Y., Guo, Q., Reetz, M.J., Whitmore, S.A., Jones, G.M., Collins, B.M., 2015. Evaluating short-and long-term impacts of fuels treatments and simulated wildfire on an old-forest species. Ecosphere 6, 1–18.
Tempel, D.J., Gutiérrez, R., Whitmore, S.A., Reetz, M.J., Stoelting, R.E., Berigan, W.J., Seamans, M.E., Peery, M.Z., 2014. Effects of forest management on California Spotted Owls: implications for reducing wildfire risk in fire-prone forests. Ecol. Appl. 24, 2089–2106.
Tucker, C.J., 1979. Red and photographic infrared linear combinations for monitoring vegetation. Remote Sens. Environ. 8, 127–150.
Valbuena, R., Hernando, A., Manzanera, J.A., Görgens, E.B., Almeida, D.R.A., Mauro, F., García-Abril, A., Coomes, D.A., 2017. Enhancing of accuracy assessment for forest above-ground biomass estimates obtained from remote sensing via hypothesis testing and overfitting evaluation. Ecol. Model. 366, 15–26.
Veraverbeke, S., Gitas, I., Katagis, T., Polychronaki, A., Somers, B., Goossens, R., 2012. Assessing post-fire vegetation recovery using red–near infrared vegetation indices: accounting for background and vegetation variability. ISPRS J. Photogramm. Remote Sens. 68, 28–39.
Verbyla, D.L., Kasischke, E.S., Hoy, E.E., 2008. Seasonal and topographic effects on estimating fire severity from Landsat TM/ETM+ data. Int. J. Wildland Fire 17, 527–534.
Viedma, O., Meliá, J., Segarra, D., García-Haro, J., 1997. Modeling rates of ecosystem recovery after fires by using landsat TM data. Remote Sens. Environ. 61, 383–398.
Vogelmann, J., Khoa, P., Lan, D., Shermeyer, J., Shi, H., Wimberly, M., Duong, H., Huong, L., 2017. Assessment of forest degradation in Vietnam using landsat time series data. Forests 8, 238.
Wang, X., Huang, H., Gong, P., Biging, G.S., Xin, Q., Chen, Y., Yang, J., Liu, C., 2016. Quantifying multi-decadal change of planted forest cover using airborne LiDAR and landsat imagery. Remote Sens. 8, 62.
White, J.C., Coops, N.C., Wulder, M.A., Vastaranta, M., Hilker, T., Tompalski, P., 2016. Remote sensing technologies for enhancing forest inventories: a review. Can. J. Remote Sens. 42, 619–641.
White, J.C., Wulder, M.A., Hermosilla, T., Coops, N.C., Hobart, G.W., 2017. A nationwide annual characterization of 25 years of forest disturbance and recovery for Canada using Landsat time series. Remote Sens. Environ. 194, 303–321.
Wulder, M.A., Masek, J.G., Cohen, W.B., Loveland, T.R., Woodcock, C.E., 2012a. Opening the archive: How free data has enabled the science and monitoring promise of Landsat. Remote Sens. Environ. 122, 2–10.
Wulder, M.A., White, J.C., Nelson, R.F., Næsset, E., Ørka, H.O., Coops, N.C., Hilker, T., Bater, C.W., Gobakken, T., 2012b. Lidar sampling for large-area forest characterization: a review. Remote Sens. Environ. 121, 196–209.
Zhao, F., Guo, Q., Kelly, M., 2012. Allometric equation choice impacts lidar-based forest biomass estimates: a case study from the Sierra National Forest, CA. Agric. For. Meteorol. 165, 64–72.
Zhao, K., Suarez, J.C., Garcia, M., Hu, T., Wang, C., Londo, A., 2017. Utility of multi-temporal lidar for forest and carbon monitoring: tree growth, biomass dynamics, and carbon flux. Remote Sens. Environ.
Zhao, X., Guo, Q., Su, Y., Xue, B., 2016. Improved progressive TIN densification filtering algorithm for airborne LiDAR data in forested areas. ISPRS J. Photogramm. Remote Sens. 117, 79–91.
Zheng, G., Moskal, L.M., 2009. Retrieving leaf area index (LAI) using remote sensing: theories, methods and sensors. Sensors 9, 2719–2745.
Zhu, Z., Woodcock, C.E., 2012. Object-based cloud and cloud shadow detection in Landsat imagery. Remote Sens. Environ. 118, 83–94.